

Probing scrambling using statistical correlations between randomized measurements

B. Vermersch,^{1,2,*} A. Elben,^{1,2} L. M. Sieberer,^{1,2} N. Y. Yao,^{3,4} and P. Zoller^{1,2}

¹Center for Quantum Physics, University of Innsbruck, Innsbruck A-6020, Austria

²Institute for Quantum Optics and Quantum Information,
Austrian Academy of Sciences, Innsbruck A-6020, Austria

³Department of Physics, University of California Berkeley, CA 94720, USA

⁴Materials Science Division, Lawrence Berkeley National Laboratory, Berkeley, CA 94720, USA

(Dated: December 14, 2024)

We present a protocol to study scrambling using statistical correlations between measurements, performed after evolving a quantum system from random initial states. We show that the resulting statistical correlations are directly related to OTOCs and can be used to probe scrambling in many-body systems. Our protocol, which does not require reversing time evolution or auxiliary degrees of freedom, can be realized in state-of-the-art quantum simulation experiments.

In recent years we have seen significant progress in understanding how thermal equilibrium can emerge in closed quantum many-body systems. It has been recognized that thermalization is driven by the spreading of entanglement [1] and the “scrambling” or delocalization of quantum information [2]. The potential of quantum dynamics described by a unitary operator $U(t)$ to entangle distant parts of a system is reflected in the complexity of Heisenberg operators $W(t) = U^\dagger(t)WU(t)$: For chaotic dynamics, even an initially “simple” and local operator W rapidly becomes complex and non-local. After a short time, $W(t)$ is delocalized and no longer commutes with an initially non-overlapping local operator V . One possibility to quantify the degree of non-commutativity, or equivalently the scrambling of $W(t)$ is given by the out-of-time order correlator (OTOC), which takes the form $O(t) = \text{Tr}(\rho W^\dagger(t)V^\dagger W(t)V)$, with ρ a quantum state. In the following, we focus on the “infinite-temperature” OTOC [3–6] for which $\rho = I/\mathcal{N}_{\mathcal{H}}$, with I the identity operator and $\mathcal{N}_{\mathcal{H}}$ the Hilbert space dimension. The time dependence of $O(t)$ can distinguish between different classes of scrambling, ranging from “fast scrambling” in models with holographic duals [7–12] and chaotic many-body spin systems [2, 5, 6, 13, 14], to “slow scrambling” characteristic of many-body localization (MBL) [3, 4, 15]. These theoretical insights raise the question of how to experimentally measure $O(t)$, despite the peculiar time order inherent in its definition. While measurement protocols for OTOCs have been devised for systems with few degree of freedoms [16–18], involving backward time evolution [19–23], or relying on auxiliary quantum systems [24], it remains a significant challenge to access $O(t)$ in experiments, when dealing with many-body systems.

In this work, we propose to diagnose scrambling via a protocol based on *statistical correlations* between measurements, performed after time-evolution from *random initial states*. This letter presents two key results, which are discussed in the context of spin systems. First, we

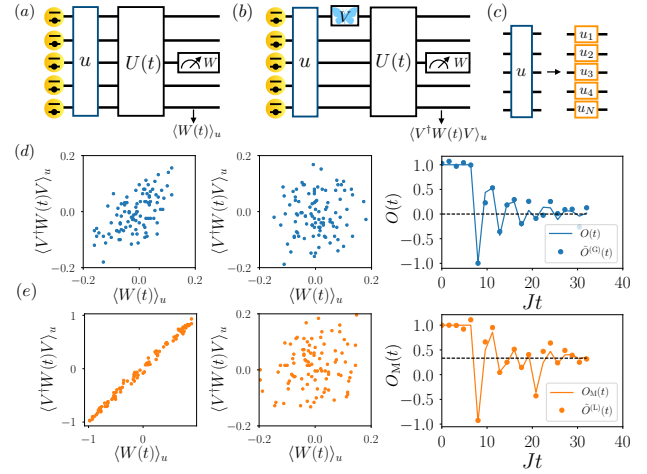


FIG. 1. *Probing scrambling via statistical correlations in a spin system.* Our protocol consists in measuring separately (a) $\langle W(t) \rangle_u$ and (b) $\langle V^\dagger W(t) V \rangle_u$ to obtain the statistical correlations $\tilde{O}^{(G)}(t)$. (c) Second protocol using local random unitaries. (d) Numerical simulations of the protocol for the kicked Ising model with parameters $h_x = J$, $h_z = 0.809J$, $JT = 1.6$, $N = 8$, and $j = 5$. The dashed lines indicate the analytical predictions (see text). The first two panels represents statistical distributions obtained with $N_u = 100$ and $N_M = 500$ projective measurements, respectively at the initial and final time of the simulation. The last panel represents the extracted unbiased correlations $\tilde{O}^{(G)}(t)$ and comparison with $O(t)$. The mismatch results from statistical errors. (e) Same as (d) with protocol based on local unitaries, extracting the modified OTOC $O_M(t)$ from the correlations $\tilde{O}^{(L)}(t)$.

show the exact equivalence between the OTOC $O(t)$, as defined above, and a measurement protocol, where the initial state is randomized with a *global* unitary operator u drawn from the circular unitary ensemble (CUE) [25] for the total many-body system. In addition, we show that our protocol can be realized in atomic quantum simulators [26–28] and with superconducting qubits [29]. Second, our discussion also motivates an experimentally simpler protocol, where the initial state is randomized with *local* random unitaries $u = u_1 \otimes u_2 \otimes \dots \otimes u_N$

* benoit.vermersch@uibk.ac.at

($u_i \in \text{CUE}$) acting on single spins $i = 1, \dots, N$. This measures a modified out-of-time ordered correlator $O_M(t)$ which, while somewhat different from $O(t)$, encodes the same physical information about scrambling. A unique feature of our protocols is that they neither require the implementation of backwards time evolution, nor the presence of an ancillary system. Finally, we demonstrate that our protocols are also robust to various forms of decoherence and experimental noise.

OTOC $O(t)$ from global random unitaries.— In the following, we present our protocol for a system \mathcal{S} of $i = 1, \dots, N$ spin 1/2 and assume W and V to be Pauli operators (which are Hermitian and unitary). As illustrated in Fig. 1(a-b), the protocol consists of the following steps: (i) Prepare the system in a product state $|k_0\rangle$ (e.g. $|k_0\rangle = |\downarrow, \dots, \downarrow\rangle$), and apply a random unitary u to obtain $|\psi_u\rangle = u|k_0\rangle$. Here, u has to be sampled from CUE [30] or more generally a unitary 2-design [31]. The randomized state $|\psi_u\rangle$ is the starting point for two independent experiments: (ii.a) Evolve the system in time with $U(t)$ and perform a measurement of the expectation value of W . Repeat steps (i) and (ii.a) N_M times with the same random unitary u to obtain $\langle W(t) \rangle_u = \langle \psi_u | W(t) | \psi_u \rangle$ (up to statistical errors, c.f. below), as illustrated in Fig. 1(a). (ii.b) In the second experiment, prepare again $|\psi_u\rangle$ and apply the unitary V . This operation is followed by the same time evolution with $U(t)$ and a measurement of W . Repeat this sequence N_M times to obtain $\langle V^\dagger W(t) V \rangle_u = \langle \psi_u | V^\dagger W(t) V | \psi_u \rangle$, as shown in Fig. 1(b). (iii) Finally, repeat steps (i) and (ii) for N_u different random unitaries, and calculate the statistical correlations between the measurement outcomes $\langle W(t) \rangle_u$ and $\langle V^\dagger W(t) V \rangle_u$ of (ii.a) and (ii.b), respectively. These correlations are quantified by a correlation coefficient

$$\tilde{O}^{(G)}(t) = \frac{\overline{\langle W(t) \rangle_u \langle V^\dagger W(t) V \rangle_u}}{\left(\overline{\langle W(t) \rangle_u^2} \overline{\langle V^\dagger W(t) V \rangle_u^2} \right)^{1/2}}, \quad (1)$$

where $\overline{\dots}$ denotes the ensemble average over random unitaries u .

Our first key result is that this correlation coefficient equals the infinite temperature OTOC

$$\tilde{O}^{(G)}(t) = O(t). \quad (2)$$

Before proving Eq. (2), we find it instructive to present in Fig. 1(d) the intuitive physical picture behind this result (for details on the simulations, see below). At $t = 0$, the measurement of $W(0) = W = \sigma_j^z$ ($j > 1$) is not affected by the operator $V = \sigma_1^z$ distinguishing the two initial states $|\psi_u\rangle$ and $V|\psi_u\rangle$. Indeed, $[V, W(0)] = 0$ and hence $\langle W(0) \rangle_u = \langle V^\dagger W(0) V \rangle_u$, implying perfect correlations and $\tilde{O}^{(G)}(0) = 1 = O(0)$ (for $N_M \rightarrow \infty$), see Fig. 1(d) left panel. At later times (middle panel), when $[V, W(t)] \neq 0$ due to the spreading of $W(t)$, the value of $\langle V^\dagger W(t) V \rangle_u$ becomes decorrelated from $\langle W(t) \rangle_u$. In the right panel, we show the time evolution of $O(t)$, and $\tilde{O}^{(G)}(t)$ extracted from the statistical correlations. In

analogy to our approach, we note that the distance between a quantum state and a copy, which is perturbed at $t = 0$ by the operator V , has been proposed to numerically detect scrambling [32, 33].

Equation (2) can be proven using the “2-design” identities of the CUE ensemble [34], which provide analytical expressions for the statistical correlations between the matrix elements of u . First, we can prove [35]

$$\begin{aligned} \overline{\langle W(t) \rangle_u \langle V^\dagger W(t) V \rangle_u} &= c \sum_{\tau=I, \text{Swap}} \text{Tr}[\tau(W(t) \otimes V^\dagger W(t) V)] \\ &= c \text{Tr}[W(t) V^\dagger W(t) V], \end{aligned} \quad (3)$$

with $c = [\mathcal{N}_{\mathcal{H}}(\mathcal{N}_{\mathcal{H}} + 1)]^{-1}$. The trace in the first line is performed over an extended Hilbert space $\mathcal{H} \otimes \mathcal{H}$, where \mathcal{H} is the Hilbert space of dimension $\mathcal{N}_{\mathcal{H}} = 2^N$, and the swap operator is $\text{Swap}|k\rangle \otimes |k'\rangle = |k'\rangle \otimes |k\rangle$ for each pair of basis states $|k\rangle = |k_1\rangle \otimes \dots \otimes |k_N\rangle$, $|k'\rangle = |k'_1\rangle \otimes \dots \otimes |k'_N\rangle$ ($|k_i\rangle, |k'_i\rangle = |\downarrow\rangle, |\uparrow\rangle$). The identities $\text{Tr}[W(t)] = 0$ for Pauli operators and $\text{Tr}[\text{Swap}(W(t) \otimes V^\dagger W(t) V)] = \text{Tr}[W(t) V^\dagger W(t) V]$ yield the second line of Eq. (3), which then proves Eq. (2) [38].

The protocol presented above to measure $O(t)$ requires an ensemble of global random unitaries which reproduces the second-order correlations of the CUE (the 2-design identities). As shown in Refs. [39–41], such global 2-designs can be realized using generic many-body Hamiltonians combined with time-dependent engineered disorder.

Modified OTOC $O_M(t)$ from local random unitaries.— Instead of applying global unitaries, we now describe a second protocol, where unitaries $u \in \text{CUE}(\mathcal{N}_{\mathcal{H}})$ are replaced by a product of local unitaries $u = u_1 \otimes \dots \otimes u_N$ ($u_i \in \text{CUE}(2)$) acting independently as random spin rotations on each site i [c.f. Fig. 1(c)]. This protocol has the advantage of being more suited for an implementation in quantum simulators with individual spin control, e.g. with trapped ions [27], Rydberg atoms [28] or superconducting qubits [29], and provides access to a variant of the OTOC denoted $O_M(t)$, which carries the same physical signatures of scrambling as $O(t)$. Note that local random unitaries have been recently implemented with high-fidelity in a trapped ion setup and used to obtain Rényi entropies from randomized measurements [40, 42].

The second version of the protocol is identical to the one outlined above. As in Eq. (1), we define the correlation coefficient $\tilde{O}^{(L)}(t)$ with the ensemble average now taken with respect to local random unitaries $u = u_1 \otimes \dots \otimes u_N$. Such correlations $\tilde{O}^{(L)}(t)$ map to a modified OTOC [35]

$$\tilde{O}^{(L)}(t) = O_M(t) \equiv \frac{\sum_{A \subseteq \mathcal{S}} \text{Tr}_A(W_A(t) [V^\dagger W(t) V]_A)}{\sum_{A \subseteq \mathcal{S}} \text{Tr}_A(W_A^2(t))}, \quad (4)$$

where the sums in Eq. (4) extend over all subsystems $A = \{i_1, \dots, i_{N_A}\}$, $N_A \leq N$, of the total system \mathcal{S} , and $X_A \equiv \text{Tr}_{\mathcal{S} \setminus A}(X)$ denotes the reduced operator of subsystem A . Hence, $\tilde{O}^{(L)}(t)$ equals a sum of infinite-temperature OTOCs of the reduced operators $W(t)_A$,

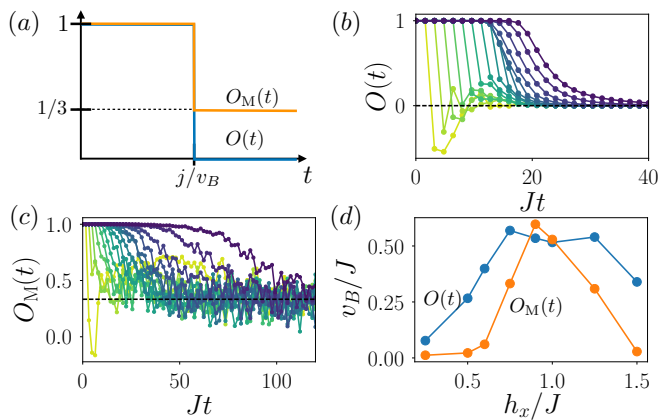


FIG. 2. $O_M(t)$ vs. $O(t)$ for chaotic dynamics. (a) Analytical predictions with ballistic chaotic dynamics governed by the butterfly velocity v_B . (b-c) In a kicked Ising model with $N = 16$ sites, representing a chaotic spin system, both $O(t)$ and $O_M(t)$, reveal the operator spreading characterized by ballistic growth with a slowly broadening front. $O_M(t)$ was estimated from $\tilde{O}^{(L)}(t)$ using $N_u = 100$ (see text). Yellow to purple curves correspond to different operator locations $j = 2, \dots, N$. The dashed lines in (b-c) indicate the analytical predictions Eq.(6). Parameters are $h_x = 0.75J$, $h_z = 0.809J$, and $JT = 1.6$. (d) Butterfly velocity v_B obtained when varying the transverse field h_x .

$(V^\dagger W(t)V)_A$, extended over all subsystems A . This structure is directly related to the tensor product structure of the applied unitaries $u = u_1 \otimes \dots \otimes u_N$.

Below we study in the detail the properties of $O_M(t)$ and show in the context of various analytical and numerical examples that it captures the essential features of the familiar $O(t)$. This is first illustrated in Fig. 1 (e), where we show that the statistical correlations $\tilde{O}^{(L)}(t) = O_M(t)$ decay as $\tilde{O}^{(G)}(t) = O(t)$ (compare to Fig. 1 (d)). Note that, as visible in the left panels and explained below, statistical errors are significantly reduced for the protocol with local unitaries.

Chaotic dynamics.— Scrambling in chaotic spin models is characterized by two key features: The support of an operator $W(t)$ that is initially localized grows ballistically $\sim v_B t$ with a “butterfly velocity” v_B , and the operator front traveling at v_B broadens diffusively [2, 5, 6]. The ballistic growth can be captured by a simple phenomenological model, which assumes that at time t the time evolution operator takes the form $U(t) = U[L(t)]_1 \otimes \dots \otimes U[L(t)]_{N/L(t)}$, where the Haar random unitaries $U[L(t)] \in \text{CUE}(2^{L(t)})$ describe scrambling on a linearly growing scale $L(t) = 1 + \text{floor}(v_B t)$. For $W = \sigma_j^z$ and $V = \sigma_1^z$, we obtain [13, 35]

$$O(t) = 1 \quad O_M(t) = 1 \quad (j > L(t)) \quad (5)$$

$$O(t) = -\frac{1}{4^{L(t)}} \quad O_M(t) = \frac{1}{3} \quad (j \leq L(t)), \quad (6)$$

in leading order in $L(t) \gg 1$. Here, $O(t)$ represents the average OTOC over the unitaries U , whereas the expres-

sion for $O_M(t)$ corresponds to the average performed separately in the numerator and denominator in Eq. (4) (this corresponds for $\tilde{O}^{(L)}(t)$ to include the sampling over U in the ensemble average \dots). As shown in Fig. 2(a), $O(t) = O_M(t) = 1$ coincide thus at short times. At the “scrambling time” $t_B = r/v_B$ ($r = j - 1$), both $O(t)$ and $O_M(t)$ exhibit a sharp drop. For $t > t_B$, $O(t)$ is exponentially suppressed while $O_M(t)$ converges to $1/3$.

These predictions are confirmed by numerical simulations of the kicked Ising model, which is an example of a chaotic spin model [5]

$$U(nT) = \left[e^{-i\frac{T}{2}(\sum_i J\sigma_i^z \sigma_{i+1}^z + h_z \sigma_i^z)} e^{-i\frac{T}{2}h_x \sum_i \sigma_i^x} \right]^n, \quad (7)$$

with n a positive integer, and T the period of the Floquet system. The results are shown in Fig. 2(b-d). Note that here and in the following, we take advantage of Eq. (4) to calculate the value of $O_M(t)$ from the statistical correlations $\tilde{O}^{(L)}(t)$, via numerical sampling of the random unitaries u [43]. As shown in panels (b-c), the evolution of $O_M(t)$ resembles the one of $O(t)$, with a linearly increasing scrambling time $t_B \sim r/v_B$ and a broadening of the curves as j increases. We also observe the long-time value of $O_M(t) \approx 1/3$, which was predicted by our phenomenological model. To complete our analysis, we extracted the butterfly velocity via a numerical fit of the OTOC decay for $j = N/2$ by a hyperbolic tangent function giving us t_B and thus v_B . In the regime of fast scrambling with transverse field $h_x \sim J$, the butterfly velocities corresponding to $O(t)$ and $O_M(t)$ share the same maximum value $\sim 0.5J$. Finally, we note that away from this maximum, the decay of $O_M(t)$ is slower than the one of $O(t)$. We attribute this difference between $O_M(t)$ and $O(t)$, which is not captured by our ballistic model, to the diffusive character of the spreading of $W(t)$ [5, 6].

MBL dynamics.— MBL is the paradigmatic example of a closed quantum system, which does not thermalize [44, 45]. As a characteristic property, the decay of $O(t)$ is *slow*: it occurs at a characteristic time which scales exponentially with the distance r between the support of W and V [3, 4], which has to be contrasted to the linear increasing $t_B \propto r$ of chaotic systems. To show that the modified OTOC $O_M(t)$ shares this property, we first use the phenomenological ℓ -bit model [46, 47], which provides an effective description of the MBL phase based on the Hamiltonian

$$H = \sum_i h_i^z \sigma_i^z + \sum_{i < j} J_{R,ij} e^{-|j-i|/\xi} \sigma_i^z \sigma_j^z, \quad (8)$$

with h_i^z random fields, $J_{R,ij}$ random interactions strengths which are taken uniformly in $[-J_z, J_z]$, and ξ the localization length. Here, we have only considered 2-body interaction terms, which is sufficient to show that MBL exhibits slow scrambling [3, 4]. With $U(t) = e^{-iHt}$, $W = \sigma_j^z$, and $V = \sigma_1^z$, one finds [3, 35]

$$O(t) = \text{sinc}\left(4J_z e^{-r/\xi} t\right) \quad O_M(t) = \frac{1 + 2O(t)}{2 + O(t)}, \quad (9)$$

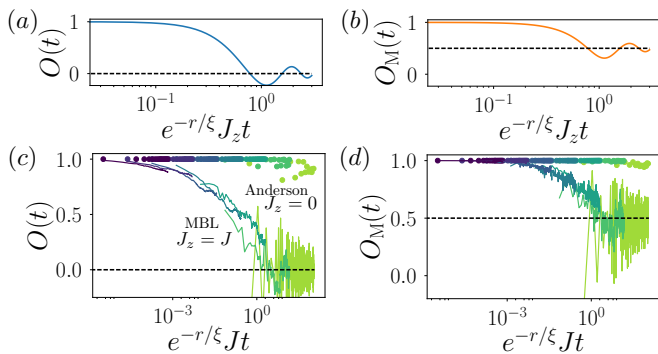


FIG. 3. $O_M(t)$ vs. $O(t)$ for MBL dynamics. (a-b) Values of $O(t)$ and $O_M(t)$ in the ℓ -bit model. (c-d) Numerical simulations for a disordered XXZ chain showing that the generic behavior and scaling of $O_M(t)$ match $O(t)$. We used $N_U = 20$ random realizations of the disorder, and $N_u = 20$ to estimate $O_M(t)$ using $\tilde{O}^{(L)}(t)$. Green to purple curves correspond to different operator locations $j = 2, \dots, N$. The lines (circles) correspond to MBL $J_z = J$ (Anderson $J_z = 0$) dynamics, respectively. The data were rescaled using a fitted localization length $\xi = 2$. Simulations were performed for $N = 8$ spins at a disorder strength of $\Delta = 10J$. The dashed lines represent the predicted long time values, $O(\infty) = 0$ and $O_M(\infty) = 1/2$ for the ℓ -bit model.

with $r = j - 1$. In the non-interacting case $J_z = 0$ (corresponding to Anderson localization) each ℓ -bit evolves independently $O(t) = O_M(t) = 1 = \text{const.}$ With interactions $J_z > 0$, the decay of both $O(t)$ and $O_M(t)$ occurs at a characteristic time $t_c = e^{r/\xi}/J_z$. This analytical result is shown in Fig. 3(a-b). Note that similar to the case of thermalizing dynamics considered above, at long times $O(t)$ tends to zero while $O_M(t)$ saturates to a finite value, here $1/2$. These results are confirmed by our numerical simulations of a disordered XXZ chain [35, 48] shown in Fig. 3(c-d). For the non-interacting case $J_z = 0$, both OTOCs values remain close to 1. In the MBL phase, the decay of $O(t)$ and $O_M(t)$ exhibits the expected exponential scaling with the distance r , and converges at long times to 0, $1/2$ respectively.

Statistical errors.—Statistical errors arise in an experiment from a finite number N_M of measurements per random unitary u to access the expectation values $\langle W(t) \rangle_u$ and $\langle V^\dagger W(t) V \rangle_u$, a finite number of random unitaries N_u used to estimate the correlation coefficients, and, additionally in disordered (random) systems, from a finite number N_U of realizations of disordered (random) time evolution. This results in deviations $\mathcal{E}^{(X)} = |[\tilde{O}^{(X)}(t)]_e - \tilde{O}^{(X)}(t)|$ ($X=R,L$) between estimated and exact correlation coefficients.

The scaling of statistical errors can be explained best in terms of the phenomenological model corresponding to Eqs. (5)-(6). Accordingly, using global unitaries, the typical value of $\langle W(t) \rangle_u \sim 1/\sqrt{2^N}$ is suppressed exponentially [35]. The number of projective measurements N_M required to access $\tilde{O}^{(G)}(t)$ up to a given error thus scales

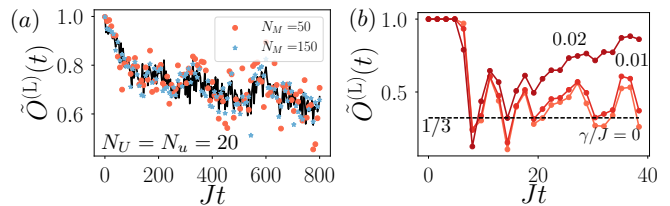


FIG. 4. *Statistical errors and the effect of decoherence.* (a) Numerics for the XXZ model with $j = 4$ and same parameters as in Fig. 3(d). For finite values of N_M (dots), we use unbiased estimators [41]. The black line represents $N_M = \infty$. (b) Decoherence vs. scrambling in the kicked Ising model. Each qubit is subject to spontaneous emission with rate γ . Other parameters are the same as in Fig. 1(e), except $N = 6$, $j = 4$, $N_M = \infty$. The effect of decoherence manifests by an increase of the correlations at long times.

as $\sim 2^N$. The protocol based on local unitaries has a crucial advantage: The typical value of the expectation values $\langle W(t) \rangle_u \sim 1/\sqrt{2^{L(t)}}$ scales instead with the effective complexity $2^{L(t)}$ of the operator, and not with the dimension 2^N of the system. Accordingly, the early-time dynamics of large chaotic systems subject to Lieb-Robinson bounds [5, 6], but also the long-time evolution of an MBL system, both of which correspond to small scrambling lengths $L(t) \ll N$, are accessible with a moderate number of measurements $\sim 2^{L(t)}$. These findings are confirmed by the numerical simulations shown in the Supplemental Material [35]. For illustration, we also show in Fig. 4(a), the estimated value of $\tilde{O}^{(L)}(t)$ in an MBL phase corresponding to the data shown in Fig. 3(d), for two simulated measurements with $N_M = 50, 150 \ll 2^N$. In both cases, statistical errors remain small over long timescales $Jt \sim 500$.

Experimental imperfections.—Our protocol is also robust against various types of experimental imperfections. For instance, the detrimental effect of the imperfect implementation of local random unitaries u is strongly suppressed when performing the ensemble average [35]. Moreover, in contrast to methods based on the reversal of time evolution [18, 23, 49], our protocol has a certain robustness against decoherence. First, depolarization noise only rescales the values of the measurements of W , while leaving statistical correlations unaltered [35]. For other sources of decoherence like spontaneous emission, the values of correlations will be affected, but in a way which can be clearly distinguished from unitary scrambling: While scrambling generically leads to a *decay* of statistical correlations, decoherence *increases* correlations. This can be understood by noting that, for a Markovian dissipative evolution, the distance between two different states always decreases with time [50]. This is illustrated in Fig. 4(b) for $\tilde{O}^{(L)}(t)$.

Conclusion and outlook.—In the present work we have provided novel protocols to measure OTOCs for spin models, based on statistical correlations between measurement outcomes obtained from random initial states.

These protocols can be implemented in state-of-the-art quantum simulation experiments on various physical platforms, in particular in Rydberg atoms, trapped ions, or superconducting qubits, which provide high repetition rates. The paradigm of extracting non-standard correlation functions of quantum many-body systems from statistical correlations points to several interesting future developments. This includes extensions to measure OTOCs for bosonic and fermionic Hubbard models [26]. In addition, beyond infinite temperature OTOCS, we present indications in the SM [35] that the protocol can be adapted to access OTOCs for thermal states. This could be used to extract the crucial temperature dependence of the Lyapunov exponents, which governs the

OTOC decay in models of high-energy physics [7–12].

ACKNOWLEDGMENTS

We thank M. Heyl, E. Altman, M. Dalmonte for discussions and comments on the manuscript. Work in Innsbruck is supported by the ERC Synergy Grant UQUAM and the SFB FoQuS (FWF Project No. F4016-N23). NYY acknowledge support from the DOE under contract PHCOMPHEP-KA24 and the Office of Advanced Scientific Computing Research, Quantum Algorithm Teams Program. For Hamiltonian simulations we used MPS and MPO techniques, implemented using ITensor (<http://itensor.org>). Simulations of master equations were based on QuTiP [51].

-
- [1] P. Calabrese and J. Cardy, *J. Stat. Mech. Theory Exp.* **2016**, 064003 (2016).
- [2] P. Hosur, X.-L. Qi, D. A. Roberts, and B. Yoshida, *J. High Energy Phys.* **2016**, 4 (2016).
- [3] R. Fan, P. Zhang, H. Shen, and H. Zhai, *Sci. Bull.* **62**, 707 (2017).
- [4] X. Chen, T. Zhou, D. A. Huse, and E. Fradkin, *Ann. Phys.* **529**, 1600332 (2017).
- [5] C. W. von Keyserlingk, T. Rakovszky, F. Pollmann, and S. L. Sondhi, *Phys. Rev. X* **8**, 021013 (2018).
- [6] A. Nahum, S. Vijay, and J. Haah, *Phys. Rev. X* **8**, 021014 (2018).
- [7] S. Sachdev and J. Ye, *Phys. Rev. Lett.* **70**, 3339 (1993).
- [8] A. Kitaev, “A simple model of quantum holography. KITP strings seminar and Entanglement 2015 program,” .
- [9] P. Hayden and J. Preskill, *J. High Energy Phys.* **2007**, 120 (2007).
- [10] S. H. Shenker and D. Stanford, *J. High Energy Phys.* **2014**, 67 (2014).
- [11] J. Maldacena, S. H. Shenker, and D. Stanford, *J. High Energy Phys.* **2016**, 106 (2016).
- [12] S. Banerjee and E. Altman, *Phys. Rev. B* **95**, 134302 (2017).
- [13] D. A. Roberts and B. Yoshida, *J. High Energy Phys.* **2017**, 121 (2017).
- [14] S. Pappalardi, A. Russomanno, B. Žunkovič, F. Iemini, A. Silva, and R. Fazio, [arXiv:1806.00022](https://arxiv.org/abs/1806.00022).
- [15] S. V. Syzranov, A. V. Gorshkov, and V. M. Galitski, [arXiv:1709.09296](https://arxiv.org/abs/1709.09296).
- [16] J. Li, R. Fan, H. Wang, B. Ye, B. Zeng, H. Zhai, X. Peng, and J. Du, *Phys. Rev. X* **7**, 031011 (2017).
- [17] M. Gärttner, J. G. Bohnet, A. Safavi-Naini, M. L. Wall, J. J. Bollinger, and A. M. Rey, *Nat. Phys.* **13**, 781 (2017).
- [18] K. A. Landsman, C. Figgatt, T. Schuster, N. M. Linke, B. Yoshida, N. Y. Yao, and C. Monroe, [arXiv:1806.02807](https://arxiv.org/abs/1806.02807).
- [19] B. Swingle, G. Bentsen, M. Schleier-Smith, and P. Hayden, *Phys. Rev. A* **94**, 040302 (2016).
- [20] G. Zhu, M. Hafezi, and T. Grover, *Phys. Rev. A* **94**, 062329 (2016).
- [21] A. Bohrdt, C. B. Mendl, M. Endres, and M. Knap, *New J. Phys.* **19**, 063001 (2017).
- [22] H. Shen, P. Zhang, R. Fan, and H. Zhai, *Phys. Rev. B* **96**, 054503 (2017).
- [23] B. Yoshida and N. Y. Yao, [arXiv:1803.10772](https://arxiv.org/abs/1803.10772).
- [24] N. Y. Yao, F. Grusdt, B. Swingle, M. D. Lukin, D. M. Stamper-Kurn, J. E. Moore, and E. A. Demler, [arXiv:1607.01801](https://arxiv.org/abs/1607.01801).
- [25] Since we consider in this work only out-of-time ordered four-point correlation functions as $O(t)$, we rely only on the second-order correlation functions of the CUE. Thus it suffices to draw u from a unitary 2-design.
- [26] I. Bloch, J. Dalibard, and S. Nascimbène, *Nat. Phys.* **8**, 267 (2012).
- [27] R. Blatt and C. F. Roos, *Nat. Phys.* **8**, 277 (2012).
- [28] A. Browaeys, D. Barredo, and T. Lahaye, *J. Phys. B At. Mol. Opt. Phys.* **49**, 152001 (2016).
- [29] J. M. Gambetta, J. M. Chow, and M. Steffen, *npj Quantum Inf.* **3**, 2 (2017).
- [30] F. Haake, *Quantum Signatures of Chaos*, Vol. 54 (Springer, 2010).
- [31] C. Dankert, R. Cleve, J. Emerson, and E. Livine, *Phys. Rev. A* **80**, 012304 (2009).
- [32] E. Levitan, F. Pollmann, J. H. Bardarson, D. A. Huse, and E. Altman, [arXiv:1702.08894](https://arxiv.org/abs/1702.08894).
- [33] X. Chen, T. Zhou, and C. Xu, [arXiv:1712.06054](https://arxiv.org/abs/1712.06054).
- [34] B. Collins and P. Śniady, *Commun. Math. Phys.* **264**, 773 (2006).
- [35] See *Supplementary Material (SM)* which presents mathematical proofs of the identities written in the main text, details on the models and numerical simulations, and which includes Refs.[35–36].
- [36] P. W. Brouwer and C. W. J. Beenakker, *J. Math. Phys.* **37**, 4904 (1996).
- [37] U. Schollwöck, *Ann. Phys. (N. Y.)* **326**, 96 (2011).
- [38] The denominator in Eq. (1), which reduces to $c\mathcal{N}_{\mathcal{H}}$, allows to reduce statistical errors for finite values of N_u and N_M .
- [39] Y. Nakata, C. Hirche, M. Koashi, and A. Winter, *Phys. Rev. X* **7**, 021006 (2017).
- [40] A. Elben, B. Vermersch, M. Dalmonte, J. I. Cirac, and P. Zoller, *Phys. Rev. Lett.* **120**, 050406 (2018).
- [41] B. Vermersch, A. Elben, M. Dalmonte, J. I. Cirac, and

- P. Zoller, *Phys. Rev. A* **97**, 023604 (2018).
- [42] T. Brydges, A. Elben, P. Jurcevic, B. Vermersch, C. Maier, B. P. Lanyon, P. Zoller, R. Blatt, and C. F. Roos, [arXiv:1806.05747](https://arxiv.org/abs/1806.05747).
- [43] F. Mezzadri, *Not. Am. Math. Soc.* **54**, 592 (2006).
- [44] D. M. Basko, I. L. Aleiner, and B. L. Altshuler, *Ann. Phys. (N. Y.)* **321**, 1126 (2006).
- [45] R. Nandkishore and D. A. Huse, *Annu. Rev. Condens. Matter Phys.* **6**, 15 (2015).
- [46] M. Serbyn, Z. Papić, and D. A. Abanin, *Phys. Rev. Lett.* **111**, 127201 (2013).
- [47] D. A. Huse, R. Nandkishore, and V. Oganesyan, *Phys. Rev. B* **90**, 174202 (2014).
- [48] A. Pal and D. A. Huse, *Phys. Rev. B* **82**, 174411 (2010).
- [49] B. Swingle and N. Y. Halpern, [arXiv:1802.01587](https://arxiv.org/abs/1802.01587).
- [50] H. P. Breuer, E. M. Laine, and J. Piilo, *Phys. Rev. Lett.* **103**, 1 (2009).
- [51] J. R. Johansson, P. D. Nation, and F. Nori, *Comput. Phys. Commun.* **184**, 1234 (2013).

Appendix A: Correspondence between statistical correlations and OTOCs

In this section, we prove Eqs. (2), (3), and (4) of the main text (MT) which relate statistical correlations to $O(t)$ and $O_M(t)$.

1. Statistical correlations between two measurements for global unitaries

Our proofs for the case of global unitaries rely on the 2-design identity

$$\begin{aligned} \overline{u_{m_1, n_1} u_{m'_1, n'_1}^* u_{m_2, n_2} u_{m'_2, n'_2}^*} &= \frac{\delta_{m_1, m'_1} \delta_{m_2, m'_2} \delta_{n_1, n'_1} \delta_{n_2, n'_2} + \delta_{m_1, m'_2} \delta_{m_2, m'_1} \delta_{n_1, n'_2} \delta_{n_2, n'_1}}{\mathcal{N}_{\mathcal{H}}^2 - 1} \\ &\quad - \frac{\delta_{m_1, m'_1} \delta_{m_2, m'_2} \delta_{n_1, n'_2} \delta_{n_2, n'_1} + \delta_{m_1, m'_2} \delta_{m_2, m'_1} \delta_{n_1, n'_1} \delta_{n_2, n'_2}}{\mathcal{N}_{\mathcal{H}}(\mathcal{N}_{\mathcal{H}}^2 - 1)}, \end{aligned} \quad (\text{A1})$$

valid for $u \in \text{CUE}(\mathcal{N}_{\mathcal{H}})$, and more generally for unitaries forming a unitary 2-design [34]. It is convenient to represent Eq. (A1) using diagrams where the contraction of the different indices are represented by lines [36]. This allows us to prove Eq. (3) of the MT, see Fig. 5(b). Here, we have introduced the notation for the initial pure density matrix $\rho_0 = |k_0\rangle\langle k_0|$.

2. Identities with local unitaries

We now consider the situation where the applied random unitaries are local $u = u_1 \otimes \cdots \otimes u_N$, where each $u_i \in \text{CUE}(d)$, d being the local Hilbert space dimension ($d = 2$ for spins). The same diagrammatic approach can be applied using a Matrix-Product-Operator (MPO) [37] representation for the operators $W(t)$ and V . This is shown in Fig. 6: each (blue) physical index is contracted following the 2-design rule shown in panel (a) while the (green) bond links remain unchanged. This can be rewritten as a sum of products of local permutations σ, τ of the physical indices, applied on two virtual copies $\rho_0 \otimes \rho_0$ and $A \otimes B$, respectively, leading to the result

$$\begin{aligned} (a) \quad \overline{u_{m_1, n_1} u_{m'_1, n'_1}^\dagger u_{m_2, n_2} u_{m'_2, n'_2}^\dagger} &= \frac{1}{\mathcal{N}_{\mathcal{H}}^2 - 1} \left[\text{Diagram 1} + \text{Diagram 2} \right] \\ &\quad + \frac{-1}{\mathcal{N}_{\mathcal{H}}(\mathcal{N}_{\mathcal{H}}^2 - 1)} \left[\text{Diagram 3} + \text{Diagram 4} \right] \\ (b) \quad \overline{\langle A \rangle_u \langle B \rangle_u} &= \overline{\left[u - \rho_0 - u^\dagger - A \right] \left[u - \rho_0 - u^\dagger - B \right]} \\ &= \frac{1}{\mathcal{N}_{\mathcal{H}}^2 - 1} \left[\text{Diagram 5} + \text{Diagram 6} \right] \\ &\quad + \frac{-1}{\mathcal{N}_{\mathcal{H}}(\mathcal{N}_{\mathcal{H}}^2 - 1)} \left[\text{Diagram 7} + \text{Diagram 8} \right] \\ &= c \sum_{\tau \in I, \text{Swap}} \overline{\tau(A \otimes B)} = c \sum_{\tau \in I, \text{Swap}} \text{Tr}[\tau(A \otimes B)] \end{aligned}$$

FIG. 5. Identities for our protocol with global unitaries. (a) Diagrammatic representation of the 2-design identities of the CUE Eq. (A1). (b) Correlations between two measurements with $A = W(t)$, $B = V^\dagger W(t)V$.

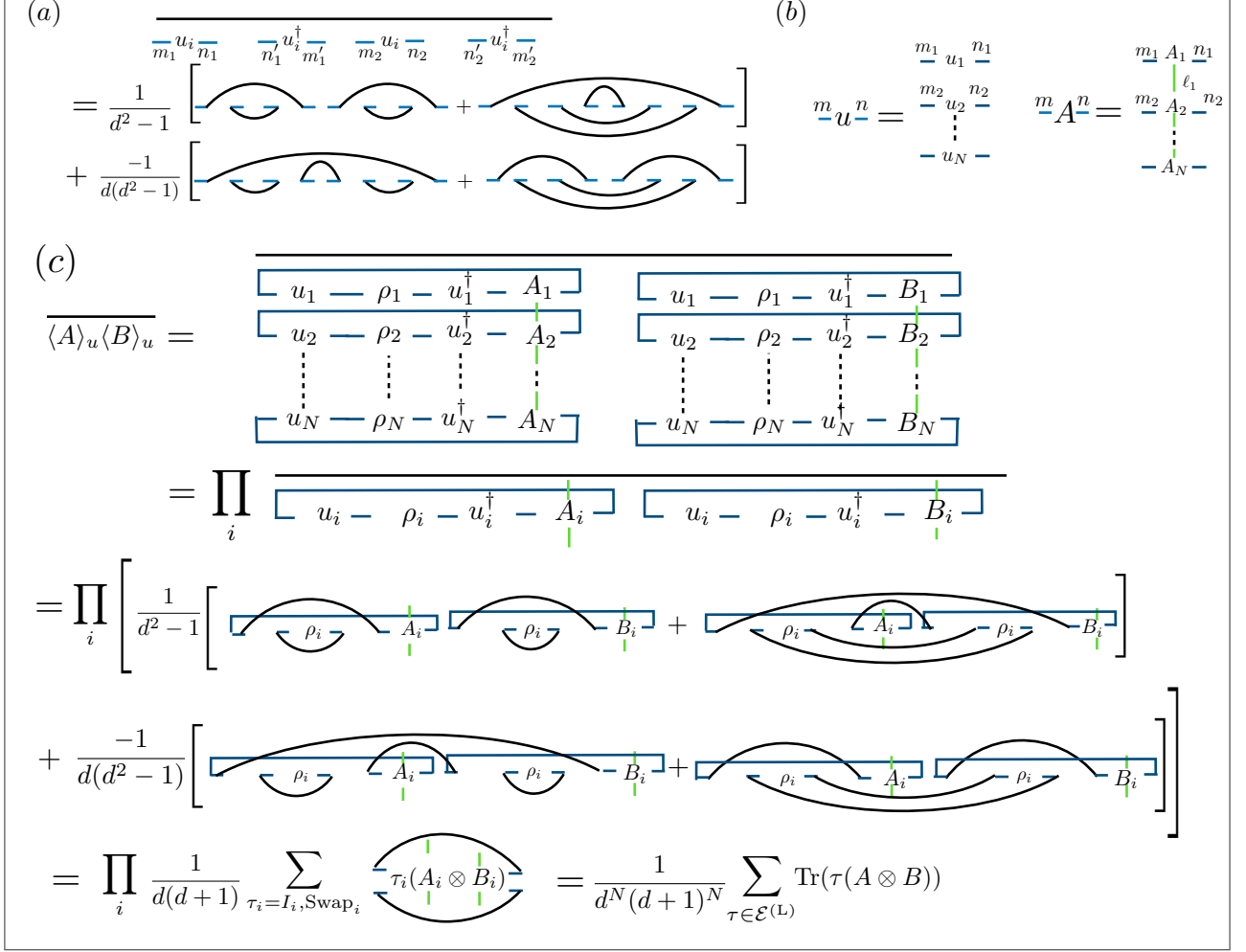


FIG. 6. *Identities for our protocol with local unitaries.* (a) Diagrammatic representation of the 2-design identities for the unitaries u_i . (b) Correlations between two measurements with $A = W(t)$, $B = V^\dagger W(t)V$.

$$\overline{\langle W(t) \rangle_u \langle V^\dagger W(t)V \rangle_u} = \frac{1}{d^N(d+1)^N} \sum_{\tau \in \mathcal{E}^{(L)}} \text{Tr}[\tau(W(t) \otimes V^\dagger W(t)V)], \quad (\text{A2})$$

and where we have used the fact that $\rho_0 = \rho_1 \otimes \dots \otimes \rho_N$ is a pure product state. The ensemble $\mathcal{E}^{(L)}$ consists of all $\tau = \otimes_i \tau_i$ products of local permutations $\tau_i = I_i, \text{Swap}_i$, with the local swap operator $\text{Swap}_i |k_i\rangle \otimes |k'_i\rangle = |k'_i\rangle \otimes |k_i\rangle$. This leads directly to the equality

$$\tilde{O}^{(L)}(t) = O_M(t) = \frac{\sum_{\tau \in \mathcal{E}^{(L)}} \text{Tr}[\tau(W(t) \otimes V^\dagger W(t)V)]}{\sum_{\tau \in \mathcal{E}^{(L)}} \text{Tr}[\tau(W(t) \otimes W(t))]} = \frac{\sum_{A \subseteq S} \text{Tr}_A(W_A(t)[V^\dagger W(t)V]_A)}{\sum_{A \subseteq S} \text{Tr}_A(W_A^2(t))}. \quad (\text{A3})$$

Appendix B: OTOCs for Haar scrambling

We now prove Eqs. (5,6) of the main text. The case $j > L(t)$ is straightforward due to the commutativity of V and W . For $j \leq L(t)$, the equality written for the OTOC $O(t)$ follows directly from the 2-design identities [c.f. Fig. 7(a)], and can also be found in Ref. [13]. We show in Fig. 7(b-c) the evaluation of $\overline{\langle W(t) \rangle_u \langle V^\dagger W(t)V \rangle_u}$, which can be

(a)

$$\begin{aligned}
O(t) &= \frac{1}{d^L} \overline{\left[U[L]_1^\dagger - W - U[L]_1 - V^\dagger - U[L]_1^\dagger - W - U[L]_1 - V \right]} \\
&= \frac{1}{d^L} \left[\frac{1}{d^{2L} - 1} \left[\overline{\left[\begin{array}{c} \text{---} \text{---} \text{---} \text{---} \text{---} \\ \curvearrowright W \curvearrowright V^\dagger \curvearrowright W \curvearrowright V \\ \text{---} \end{array} \right]} + \overline{\left[\begin{array}{c} \text{---} \text{---} \text{---} \text{---} \text{---} \\ \curvearrowright W \curvearrowright V^\dagger \curvearrowright W \curvearrowright V \\ \text{---} \end{array} \right]} \right] \\
&+ \frac{-1}{d^L(d^{2L} - 1)} \left[\overline{\left[\begin{array}{c} \text{---} \text{---} \text{---} \text{---} \text{---} \\ \curvearrowright W \curvearrowright V^\dagger \curvearrowright W \curvearrowright V \\ \text{---} \end{array} \right]} + \overline{\left[\begin{array}{c} \text{---} \text{---} \text{---} \text{---} \text{---} \\ \curvearrowright W \curvearrowright V^\dagger \curvearrowright W \curvearrowright V \\ \text{---} \end{array} \right]} \right] \\
&= \frac{-1}{d^{2L} - 1}
\end{aligned}$$

(b)

$$\begin{aligned}
\overline{\langle W(t) \rangle_u \langle V^\dagger W(t) V \rangle_u} &= \overline{\left[U[L]_1 - \rho[L]_1 - U[L]_1^\dagger - W \right] \left[U[L]_1 - \rho'[L]_1 - U[L]_1^\dagger - W \right]} \\
&= \frac{1}{d^{2L} - 1} \left[\overline{\left[\begin{array}{c} \text{---} \text{---} \text{---} \text{---} \text{---} \\ \curvearrowright \rho[L]_1 \curvearrowright W \curvearrowright \rho'[L]_1 \curvearrowright W \\ \text{---} \end{array} \right]} + \overline{\left[\begin{array}{c} \text{---} \text{---} \text{---} \text{---} \text{---} \\ \curvearrowright \rho[L]_1 \curvearrowright W \curvearrowright \rho'[L]_1 \curvearrowright W \\ \text{---} \end{array} \right]} \right] \\
&+ \frac{-1}{d^L(d^{2L} - 1)} \left[\overline{\left[\begin{array}{c} \text{---} \text{---} \text{---} \text{---} \text{---} \\ \curvearrowright \rho[L]_1 \curvearrowright W \curvearrowright \rho'[L]_1 \curvearrowright W \\ \text{---} \end{array} \right]} + \overline{\left[\begin{array}{c} \text{---} \text{---} \text{---} \text{---} \text{---} \\ \curvearrowright \rho[L]_1 \curvearrowright W \curvearrowright \rho'[L]_1 \curvearrowright W \\ \text{---} \end{array} \right]} \right] \\
&= \frac{1}{d^{2L} - 1} \left[d^L \overline{\left[\begin{array}{c} \text{---} \text{---} \text{---} \text{---} \text{---} \\ \text{---} u_1 - \rho_1 - u_1^\dagger - V - u_1 - \rho_1 - u_1^\dagger - V^\dagger \text{---} \\ \text{---} \end{array} \right]} - 1 \right]
\end{aligned}$$

(c)

$$\begin{aligned}
\text{butterfly} &= \frac{1}{d^2 - 1} \left[\overline{\left[\begin{array}{c} \text{---} \text{---} \text{---} \text{---} \\ \curvearrowright \rho_1 \curvearrowright V \curvearrowright \rho_1 \curvearrowright V^\dagger \\ \text{---} \end{array} \right]} + \overline{\left[\begin{array}{c} \text{---} \text{---} \text{---} \text{---} \\ \curvearrowright \rho_1 \curvearrowright V \curvearrowright \rho_1 \curvearrowright V^\dagger \\ \text{---} \end{array} \right]} \right] \\
&+ \frac{-1}{d(d^2 - 1)} \left[\overline{\left[\begin{array}{c} \text{---} \text{---} \text{---} \text{---} \\ \curvearrowright \rho_1 \curvearrowright V \curvearrowright \rho_1 \curvearrowright V^\dagger \\ \text{---} \end{array} \right]} + \overline{\left[\begin{array}{c} \text{---} \text{---} \text{---} \text{---} \\ \curvearrowright \rho_1 \curvearrowright V \curvearrowright \rho_1 \curvearrowright V^\dagger \\ \text{---} \end{array} \right]} \right] \\
&= \frac{d - 1}{d^2 - 1}
\end{aligned}$$

FIG. 7. Proof of Eqs. (6) of the MT using a diagrammatic approach. In panels (a-b), the ensemble average is performed over the unitaries U leading to the contractions of the red indices. In panel (c), the ensemble average is taken with respect to the unitaries u_1 with the contracted indices shown in blue.

adapted to derive $\overline{\langle W(t) \rangle_u^2}$ by replacing V by the identity matrix. Since u is a product of local random unitaries, $u\rho_0 u^\dagger$ is still a product state. To evaluate $O(t)$ and $O_M(t)$, it is convenient to group $u\rho_0 u^\dagger$ into factors pertaining to subsystems of size $L(t)$, and we write $u\rho_0 u^\dagger = \rho[L(t)]_1 \otimes \cdots \otimes \rho[L(t)]_{N/L(t)}$ and $\rho'[L(t)]_1 = V\rho[L(t)]_1 V^\dagger$.

Appendix C: OTOCs for many body localization

To describe analytically the behavior of OTOCs in the MBL phase [3, 4], we consider the ℓ -bit model with time evolution $U(t) = \exp(-iHt)$ described by the Hamiltonian

$$H = \sum_i h_i^z \sigma_i^z + \sum_{i < j} J_{i,j} \sigma_i^z \sigma_j^z, \quad (\text{C1})$$

where h_i^z are random fields which as we show below have no effect on the OTOC, $J_{ij} = J_{R,ij} \exp(-|j-i|/\xi)$, $J_{R,ij}$ a random interaction amplitude with probability distribution $f(J_{R,ij})$ which we assume uniform in $[-J_z, J_z]$, and ξ the localization length. We study the behavior of the OTOCs for the operators $W = \sigma_j^x$, and $V = \sigma_1^x$. In the Anderson case $J_z = 0$, each ℓ -bit evolves independently, and we have $O(t) = O_M(t) = 1$.

1. Single disorder realization

We now address the general MBL case $J_z > 0$ and first consider a single disorder realization of the interaction matrix (J_{ij}), writing the Heisenberg operators as

$$\begin{aligned} W(t) &= \sigma_j^x \exp(-2ith_j^z \sigma_j^z) \exp(-2it \sum_{i \neq j} J_{ij} \sigma_i^z \sigma_j^z) \\ V^\dagger W(t) V &= \sigma_j^x \exp(-2ith_j^z \sigma_j^z) \exp(-2it \sum_{i \neq j} J_{ij} c_i \sigma_i^z \sigma_j^z), \end{aligned} \quad (\text{C2})$$

with $c_{i \neq 1} = 1$, $c_1 = -1$. We then obtain

$$O(t) = \frac{1}{d^N} \text{Tr}(\exp(-4it J_{1j} \sigma_1^z \sigma_j^z)) = \cos(4J_{1j}t), \quad (\text{C3})$$

as already shown in Ref. [3, 4]. We now evaluate $O_M(t)$ using the first expression given in Eq. (A3). We first perform the trace operation with respect to the site j

$$\begin{aligned} \text{Tr}_j [(I_j + \text{Swap}_j)(W(t) \otimes W(t))] &= 2 \cos \left(2t \sum_{i \neq j} J_{ij} (\sigma_i^z - \tilde{\sigma}_i^z) \right) \\ \text{Tr}_j [(I_j + \text{Swap}_j)(W(t) \otimes V^\dagger W(t) V)] &= 2 \cos \left(2t \sum_{i \neq j} J_{ij} (\sigma_i^z - c_i \tilde{\sigma}_i^z) \right), \end{aligned} \quad (\text{C4})$$

with $\tilde{\sigma}_i^\beta$ ($\beta = x, y, z$) the set of Pauli matrices in the ‘‘copy’’ Hilbert space \mathcal{H}_i associated to site i . We can then calculate the trace over the remaining sites, for instance:

$$\begin{aligned} \text{Tr}_k \left[(I_k + \text{Swap}_k) \cos \left(2t \sum_{i \neq j} J_{ij} (\sigma_i^z - \tilde{\sigma}_i^z) \right) \right] &= [4 \cos(2t J_{kj})^2 + 2] \cos \left(2t \sum_{i \neq k, j} J_{ij} (\sigma_i^z - \tilde{\sigma}_i^z) \right) \\ \text{Tr}_k \left[(I_k + \text{Swap}_k) \cos \left(2t \sum_{i \neq j} J_{ij} (\sigma_i^z - c_i \tilde{\sigma}_i^z) \right) \right] &= [4 \cos(2t J_{kj})^2 + 2 \cos(2(1 - c_k) J_{kj}t)] \cos \left(2t \sum_{i \neq k, j} J_{ij} (\sigma_i^z - \tilde{\sigma}_i^z) \right). \end{aligned} \quad (\text{C5})$$

All the factors which enter in the numerator and in the denominator in Eq. (A3) are identical, except for the position $k = 1$ of the V operator. This leads to

$$O_M(t) = \frac{4 \cos(2J_{1j}t)^2 + 2 \cos(4J_{1j}t)}{4 \cos(2J_{1j}t)^2 + 2} = \frac{2 \cos(4J_{1j}t) + 1}{\cos(4J_{1j}t) + 2}. \quad (\text{C6})$$

2. Averaged OTOCs

Considering now a distribution of the random realizations of J_{ij} , $O_M(t)$ is now obtained from Eq. (A3), where the numerator and the denominator are replaced by their ensemble average (see text). Repeating the above derivation, replacing each cosine contribution by the average

$$\cos(\alpha J_{ij}t) \rightarrow \int_{-J_z}^{J_z} dJ_{R,ij} \cos(\alpha J_{R,ij} e^{-|j-i|/\xi} t), \quad (\text{C7})$$

we obtain Eq. (9) of the MT.

Appendix D: Numerical simulation of spin models

In this section, we give details on the numerical simulations presented in the main text. For both models we used open boundary conditions.

1. Simulations of the kicked Ising model

To simulate scrambling dynamics, we use the kicked Ising model and follow the notations from Ref. [5]

$$U(t = nT) = \left[\exp \left(-i \frac{T}{2} \left[\sum_i J \sigma_i^z \sigma_{i+1}^z + h_z \sum_i \sigma_i^z \right] \right) \exp \left(-i \frac{T}{2} h_x \sum_i \sigma_i^x \right) \right]^n, \quad (\text{D1})$$

with n a positive integer, and T the period of the Floquet system.

For Fig. 4 (b) of the main text related to decoherence, the dynamics was calculated from the Lindblad master equation

$$\begin{aligned} \dot{\rho}(t) &= -i[H(t), \rho(t)] + \gamma \sum_i \mathcal{L}[\sigma_i^-](\rho(t)) \\ H(t \in [(n-1)T, nT - \frac{T}{2}]) &= h_x \sum_i \sigma_i^x \\ H(t \in [nT - \frac{T}{2}, nT]) &= J \sum_i \sigma_i^z \sigma_{i+1}^z + \sum_i h_z^i \sigma_i^z \\ \mathcal{L}[\sigma_i^-](\rho) &= \frac{1}{2} [2\sigma_i^- \rho \sigma_i^+ - \rho \sigma_i^+ \sigma_i^- - \sigma_i^+ \sigma_i^- \rho], \end{aligned} \quad (\text{D2})$$

with initial condition $\rho(0) = \rho_0$.

2. Simulations of the disordered XXZ model

To describe the OTOCs in the MBL dynamics [3], we consider the XXZ model

$$H = \sum_i [J (\sigma_i^+ \sigma_{i+1}^- + \sigma_i^- \sigma_{i+1}^+)] + J_z \sigma_i^z \sigma_{i+1}^z + \sum_i h_z^i \sigma_i^z, \quad (\text{D3})$$

with h_z^i sampled from a uniform distribution $[-\Delta, \Delta]$.

Appendix E: Numerical study of statistical errors

The numerical study of statistical errors for the scrambling model [Eq. (4) MT] is shown in Fig. 8. We consider the worst-case scenario $j < L$ with small correlations $\tilde{O}^{(G,L)}(t)$ to be extracted. The results confirm the statements written in the MT: (a) with global unitaries, the required number of projective measurements N_M scales as 2^N . (c) with local unitaries, $N_M \sim 2^L$ is generically much smaller.

As shown in Fig. 8(b,d), statistical errors for $N_M \rightarrow \infty$ decrease as $1/\sqrt{N_u}$ with growing number of applied random unitaries N_u , independently of $L(t)$ and N . We found the same behavior when increasing N_U .

Appendix F: Limited reproducibility of generated random unitaries

In this section, we analyze the robustness of our protocol with respect to imperfections in the generation of random unitaries. Specifically, we consider that $\langle W(t) \rangle_u$ is obtained from a random unitary matrix $u = u_1 \otimes \cdots \otimes u_N$, with $u_i \in \text{CUE}(2)$, while the second measurement $\langle V^\dagger W(t) V \rangle_{u'}$ is obtained from a slightly different unitary $u' = u'_1 \otimes \cdots \otimes u'_N$ which we write as

$$u'_i = R_{iz}(\theta_{i1}) R_{iy}(\theta_{i2}) R_{iz}(\theta_{i3}) u_i. \quad (\text{F1})$$

Here, $R_{i\gamma}$ denote single qubit rotations for spin i along the γ axis, and θ_{in} are assumed to be random angles drawn uniformly in $[-\theta, \theta]$, which represent the unwanted mismatch between the unitaries u and u' .

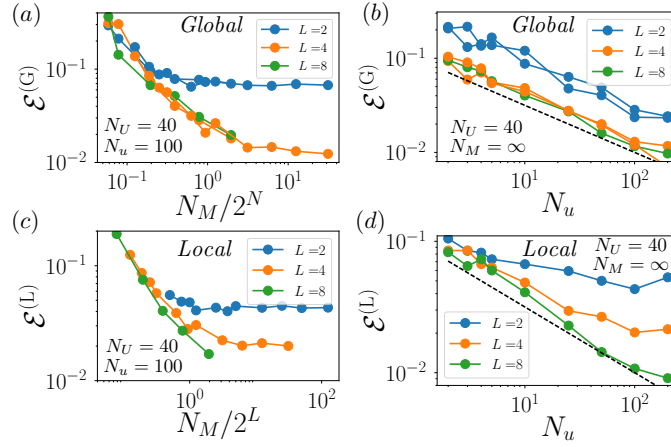


FIG. 8. *Statistical errors* (a-b) Scalings of the error $\mathcal{E}^{(G)}$ in the estimation of $\tilde{\mathcal{O}}^{(G)}(t)$ as a function of N_M (a) and N_u (b). We used two values of $N = 4, 8$. (c-d) Same as (a-b) for $\tilde{\mathcal{O}}^{(L)}(t)$ (here the simulations are independent of N). The final plateaus in (a),(c),(d) are due to the finite values of $N_u N_U$. The dashed lines in (b-d) show $0.1/\sqrt{N_u}$.

1. Analytical understanding of the robustness of the protocol

To show that our protocol is robust against such imperfections, we calculate the estimator of the OTOC, obtained from

$$\tilde{\mathcal{O}}^{(L)}(t) = \frac{\overline{\langle W(t) \rangle_u \langle V^\dagger W(t) V \rangle_{u'}}}{\sqrt{\overline{\langle W(t) \rangle_u^2} \overline{\langle V^\dagger W(t) V \rangle_{u'}^2}}}. \quad (\text{F2})$$

In first order in θ_{in} , we can write $u' = u + \sum_{i,n} \theta_{in} A_{in}$, with $A_{in} = R'_{in}(0)u$. This leads to

$$\overline{\langle W(t) \rangle_u \langle V^\dagger W(t) V \rangle_{u'}} = \overline{\langle W(t) \rangle_u \langle V^\dagger W(t) V \rangle_u} + \sum_{i,n} \overline{\theta_{in}} \overline{\langle W(t) \rangle_u \text{Tr}([u \rho_0 A_{in}^\dagger + A_{in} \rho_0 u^\dagger] V^\dagger W(t) V)}, \quad (\text{F3})$$

where the second term vanishes due to $\overline{\theta_{in}} = 0$. Similarly, we obtain $\overline{\langle V^\dagger W(t) V \rangle_{u'}} = \overline{\langle V^\dagger W(t) V \rangle_u}$, still valid in first order in θ_{in} , and thus $\tilde{\mathcal{O}}^{(L)}(t) = \tilde{\mathcal{O}}^{(L)}(t)$. Our protocol is thus robust to first order in θ against imperfections of the generated unitaries. As shown below, the quadratic contribution scales linearly with the characteristic size $L(t)$ of the operator $W(t)$.

2. Numerical example

We now consider a numerical example for the model of scrambling presented in the MT. To assess the robustness of statistical correlations, we consider $j > L(t)$ so that the exact OTOC is $\tilde{\mathcal{O}}^{(L)}(t) = 1$, and imperfect generated unitaries as written above.

The numerical results are shown in Fig. 9 and confirm our analytical treatment: there is no linear correction in θ in the error \mathcal{E} of the estimated OTOC. However, the error scales as $\theta^2 L$, showing that the quadratic contribution does not vanish.

Appendix G: Robustness against the depolarizing channel

In the presence of depolarizing noise [23], the realized quantum state can be written as

$$\rho_f = (1-p)U_{\text{tot}}(t)\rho_0 U_{\text{tot}}^\dagger(t) + \frac{pI}{d^N}, \quad (\text{G1})$$

with $0 < p < 1$ the depolarization probability, $U_{\text{tot}}(t)$ the desired time-evolution unitary operator. This translates to the two measurements outcomes [for the sequence shown in Fig. 1 MT with $U_{\text{tot}}(t) = U(t)u$ (a) and $U_{\text{tot}}(t) = U(t)Vu$

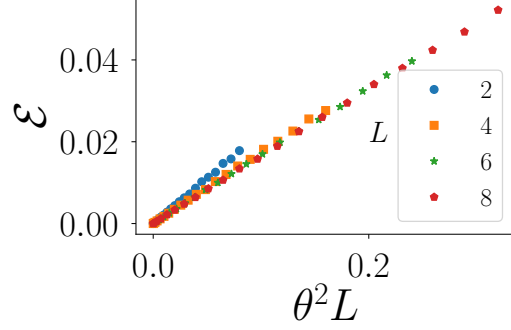


FIG. 9. Robustness of the protocol with respect to a mismatch between generated random unitaries. The error \mathcal{E} is plotted as a function of the scaling parameter $\theta^2 L$, for $L = 4, 6, 8$ and $0 < \theta < 0.2$. Note that all data points, the error is below 6%.

(b)]

$$\begin{aligned}\langle W(t) \rangle'_u &= (1-p)\langle W(t) \rangle_u \\ \langle V^\dagger W(t) V \rangle'_u &= (1-p)\langle V^\dagger W(t) V \rangle_u.\end{aligned}\tag{G2}$$

Hence, the two measurements are simply rescaled, and the statistical correlations are not affected by the depolarizing channel.

Appendix H: Thermal OTOCs from global unitaries

In this section, we show how our protocol can be extended to include finite temperature corrections to $O(t)$. To this end, we employ a high-temperature expansion of the thermal density matrix $\rho_\beta = \exp(-\beta H)/Z$, with H being the many-body Hamiltonian of the system of interest $Z = \text{Tr}(\exp(-\beta H))$ and β the inverse temperature. Specifically, we are interested in the canonical finite temperature OTOC

$$O[\rho_\beta](t) = \text{Tr}(\rho_\beta W(t) V W(t) V),\tag{H1}$$

with ρ_β a thermal density matrix and a symmetrized variant, introduced in Ref. [11],

$$O_S[\rho_\beta](t) = \text{Tr}(\rho_\beta^{1/4} W(t) \rho_\beta^{1/4} V \rho_\beta^{1/4} W(t) \rho_\beta^{1/4} V).\tag{H2}$$

Here, and in the following, we assume $W(t)$ to be hermitian, V to be hermitian and unitary, and all operators W, V, H to be traceless (which is the case for the spin models considered in the main text). We employ a high-temperature expansion of $\rho_\beta \sim (I - \beta H)/\mathcal{N}_\mathcal{H} + \mathcal{O}(\beta^2)$. To first order in β we find

$$O[\rho_\beta](t) = O(t) - \frac{\beta}{\mathcal{N}_\mathcal{H}} \text{Tr}(H W(t) V W(t) V) + \mathcal{O}(\beta^2),\tag{H3}$$

and

$$O_S[\rho_\beta](t) = O(t) - \frac{\beta}{2\mathcal{N}_\mathcal{H}} (\text{Tr}(H W(t) V W(t) V) + \text{Tr}(H V W(t) V W(t))) + \mathcal{O}(\beta^2).\tag{H4}$$

We now introduce the statistical correlations

$$\tilde{C}(t) = \overline{\langle W(t) \rangle_u \langle V W(t) V \rangle_u \langle H \rangle_u},\tag{H5}$$

with u global random unitaries of the CUE and $\langle A \rangle_u = \langle \psi_u | A | \psi_u \rangle$. Using the 3-design properties of the CUE, we obtain

$$\tilde{C}(t) = c' \sum_{\tau \in S_3} \text{Tr}(\tau[W(t) \otimes V W(t) V \otimes H]),\tag{H6}$$

with $c' = [\mathcal{N}_\mathcal{H}(\mathcal{N}_\mathcal{H} + 1)(\mathcal{N}_\mathcal{H} + 2)]^{-1}$. This can be rewritten as

$$\tilde{C}(t) = c' (\text{Tr}(H W(t) V W(t) V) + \text{Tr}(H V W(t) V W(t))).\tag{H7}$$

Using Eqs. (H4)-(H7), and $O(t) = \tilde{O}^{(G)}(t)$, we obtain

$$O_S[\rho_\beta](t) = \tilde{O}^{(G)}(t) - \frac{\beta}{2c\mathcal{N}_{\mathcal{H}}}\tilde{C}(t), \quad (\text{H8})$$

which shows that, in contrast to the asymmetric form $O(t)$, $O_S[\rho_\beta](t)$ can be extracted from the statistical correlations $\{\tilde{O}^{(G)}(t), \tilde{C}(t)\}$. This provides a first indication that thermal OTOCs may be accessible experimentally using such extension of our protocols. The additional requirement compared to the measurement of $O(t)$ is the ability to access the energy $\langle H \rangle_u$ of random initial states.